Investigation of Bending Sensitivity in Partially Doped Core Fiber for Sensing Applications

Siamak Dawazdah Emami, Hairul A. Abdul-Rashid, Fatemeh Zahra Zahedi, Mukul Chandra Paul, Shyamal Das, Mrinmay Pal, and Sulaiman Wadi Harun

***Abstract*— A fiber based high sensitive bend sensor is proposed and demonstrated using a uniquely designed partially doped core fiber (PDCF). The fabrication method of PDCF with two core regions, namely an undoped outer region with a diameter of ∼9.5 μm encompassing a doped, inner core region with a diameter of 4.00 μm is explained. The mechanism of bending effect in proposed PDCF and the experimental setup for amplified spontaneous emission (ASE) based sensor and fiber laser based sensor is illustrated. For ASE sensor, the higher ASE power level loss as the spooling radius is reduced from 20 to 3 cm is measured. The gain peak shift to shorter wavelength with respect to the decrease of the spooling radius from 20 to 3 cm due to higher bending loss at smaller bending radius is observed. The results are in agreement with overlap factor variation of PDCF. As expected from ASE peaks variation, the fiber laser sensor spectral operation is changed from 1539 to 1530 nm range. This phenomenon is due to higher mode field diameter of longer wavelength and result of optical filtering at longer wavelengths. The experimental results showed the output of the ASE is also highly stable, with no observable variation in the power output over a measurement period of 1 h. The PDCF is also temperature insensitive.**

***Index Terms*— Optical sensors, partially doped core fiber, fiber laser sensor.**

I. Introduction

THE applications of fiber optic sensors (FOS) on forces, pressure, temperature, vibration, frequencies and other acoustic parameters measurement have progressed rapidly in recent years. Optical fiber sensors are used in difficult measurement situations, where conventional sensors are not well suited in a particular environment [1]–[4]. non-electric nature of optical fiber sensors make them suitable for operations in hazardous environments [5]. Compact and lightweight, wide bandwidth, efficient multiplexing on a single fiber network, immunity from electromagnetic interference (EMI), and cost effective are the other advantages of fiber optic sensors [5].

One of the most popular technological developments in the sensor and optical telecommunications fields is doped fiber sensors. Doped fiber macro bend sensors are relatively few and used to measure parameters such as temperature, deformation, and pressure [6]–[11]. A fiber laser pressure sensor utilizing erbium doped fiber as the amplification medium in a linear cavity resonator was reported earlier in [8]. The fiber laser pressure sensor has characteristics of simple configuration, low threshold power, stable output power, and high signal to noise ratio. Another example of macro bent doped-fiber sensor is the distributed temperature sensor. It employs a distributed erbium doped fiber amplifier (EDFA) and utilizes the temperature dependence of the gain and of the amplified spontaneous emission in an EDFA [9]. In addition, Depressed Cladding Erbium Doped Fiber (DC-EDF) is a special fiber that uses the bending mechanism to obtain optical amplification in S-Band. The application of this fiber as new types of optical sensing systems has been presented by considering the DC-EDF amplification and lasing bend dependence characteristics [10]. For the case of DC-EDF, the peak wavelength of the amplified spontaneous emission (ASE) spectrum shifts as the bending radius decreases [11]. This will allow a simple detection system to be built, where a filter can be inserted to coincide the peak wavelength, which then allows for the measurement of the output power against the bending radius.

Despite the different advantages of the macro bent doped-fiber sensor, there are still some limitations. This includes the low bending radius threshold for sensing make the fiber fragile. Another limitation is the selective sensitivity at a particular bending radius and wavelength. The sensor has high sensitivity for bending radius lower than the threshold radius and low sensitivity for bending radius higher than the threshold, which makes the sensor less effective.

Influence of the Erbium distribution profile (ETD) on the EDFA behavior observed significant gain differences in active fibers. It is found that in PDCF higher overlapping parameter turns out gain enhancement in active fiber [12]–[14]. The mode field distribution for PDCF in comparison with normal doped fiber falls outside the doping area at the bending situation and suffers more due to active bending loss [15]. Temperature insensitive, with only a minor variation is the other factor of proposed fiber [16].

Manuscript received September 7, 2013; revised November 20, 2013; accepted November 22, 2013. Date of publication December 5, 2013; date of current version February 21, 2014. The associate editor coordinating the review of this paper and approving it for publication was Dr. Anna G. Mignani.

S. D. Emami and S. W. Harun are with the Department of Electrical Engineering. Faculty of Engineering, University of Malaya, Kuala Lumpur 50603, Malaysia (e-mail: s.d.emami@gmail.com).

H. A. Abdul-Rashid is with the Faculty of Engineering, Multimedia University, Cyberjaya 63100, Malaysia (e-mail: hairul@mmu.edu.my).

F. Z. Zahedi is with the Department of Electrical Engineering, Faculty of Electrical and Computer Engineering, Shahid Beheshti University, Tehran 19839, Iran (e-mail: fa.zahedi66@gmail.com).

M. C. Paul, S. Das, and M. Pal are with the Fiber Optics and Photonics Division, Central Glass and Ceramic Research Institute, Council of Scientific and Industrial Research, Kolkata 700 032, India (e-mail: paulmukul@hotmail.com; dshyamal@cgcri.res.in; mpal@cgcri.res.in).

Color versions of one or more of the figures in this paper are available online at http://ieeexplore.ieee.org.

Digital Object Identifier 10.1109/JSEN.2013.2294244

Recently we present experimentally the ASE bend sensor using a PDCF. Spooling the PDCF decreases the peak power, from an average of −57.0 dBm to −61.8 dBm at spooling diameters of 10 cm to 2 cm. The output of the ASE is also highly stable, with no observable variation in the power output over a measurement period of one hour. The PDCF is also temperature insensitive, with only a minor variation of about ∼0.005 dBm/°C measured, thus reducing the effects of cross-sensitivity [16].

In this paper we investigate the bending sensitivity of PDCF particularly for sensing applications based on amplifier and laser sensors. The ASE profile of an amplifier using the PDCF, doped with Erbium, is observed to vary with the bending radius. In another setup, a fiber laser employing the PDCF as the active medium also has a lasing wavelength varying with the bending radius. In the first part of the paper, Fabrication and spectroscopic of PDCF is described. The amplifier and fiber laser configurations using the PDCF sensor is presented at next part. The mechanism of macro bending effect on PDCF is also presented. Next, the experimental results of the PDCF amplifier and fiber laser PDCF sensor are demonstrated. It is shown that using ASE based sensor, the ASE power level will change from −38.0 dBm to −61.8 dBm as the spooling radius is reduced from 20 cm to 3 cm is measured. The loss variation of 30 dB for 8 m PDCF length obtained for 1540 nm signal in the range from 4 to 20 cm bending radius is a very good value when compared with the best bending sensor. As expected from amplifier sensor peak variation, the mode lock fiber laser sensor spectral operation is changed from 1539 nm to 1530 nm range. Numerical and experimental results shown that the proposed sensor has high sensitivity, high dynamic range, and wide bandwidth that make it suitable to monitor static parameters such as force, pressure, and displacement.

II. Fabrication and Spectroscopic of PDCF

A special design of Partially Doped Core Fiber (PDCF) with double layers core structure was done by the conventional modified chemical vapor deposition (MCVD) process followed by solution doping technique. The un-doped photosensitive layer is based on germano-silicate glass. The desired thickness and RI of the un-doped photosensitive layer was obtained after optimisation of the flow of $SiCl_4$ and $GeCl_4$ vapour in a mixture of gaseous reactants. The inner clad of SiO_2-P_2O_5-F composition having the same refractive index of silica was made by adjustment of the flow of phosphoryl chloride ($POCl_3$) and dichlorodifluoromethane (CCl_2F_2) with respect to the flow of $SiCl_4$. After cladding layer, un-doped SiO_2-GeO_2 photosensitive layer was deposited within 20/17 mm silica tube by the MCVD process. A pure silica glass tube with thickness of 1.5 mm was used for deposition of a single porous un-sintered SiO_2 soot layer to make the preform while maintaining a suitable deposition temperature at around 1450 °C–1475 °C. The deposited porous SiO_2 layer was dipped into an alcoholic solution of a mixture of suitable strength of $AlCl_3$ $6H_2O$, $ErCl_3$ $6H_2O$ for about one hour to achieve efficient doping. After the completion of solution soaking, dehydration and oxidation processes were performed at temperature around 900 °C–1000 °C. Sintering of un-sintered layers was carried out using the conventional MCVD technique by slowly increasing the temperature from 1500 to 2000 °C. Following the completion of sintering as well as oxidation, the tube was slowly collapsed to transform it into optical preform. The fiber was drawn from such fabricated preform at temperature of 2050 °C into a spool of optical bare fiber with on–line dual coating resin.

TABLE I
Proposed Design of Partially Erbium Doped Core Er Fiber (PDCF)

Parameters	Value
Composition of photosensitive layer	SiO_2-GeO_2
Composition of central doped core layer	SiO_2-Al_2O_3-Er_2O_3
Thickness of photosensitive layer	2.75 micron
Diameter of doped core layer	4.0 micron
Refractive index of undoped photosensitive and central doped layers	1.45565 at 633 nm
Erbium ions doping levels	400 ppm

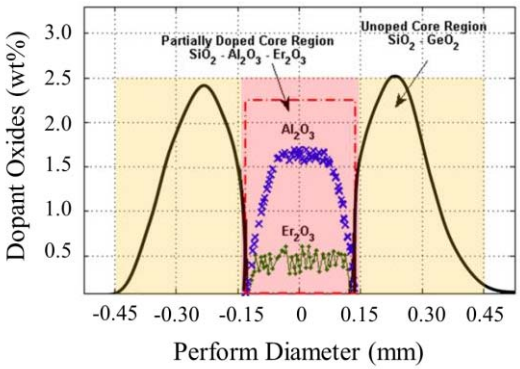

Fig. 1. Electron probe micro analyses of PDCF.

The desired thickness around 2.75 micron of un-doped photosensitive layer and refractive index (RI) of the ring core was obtained after optimisation of the flow of $SiCl_4$ and $GeCl_4$ vapour in a mixture of gaseous reactants. The inner clad of SiO_2-P_2O_5-F composition having the same refractive index of silica was made by adjustment of the flow of $POCl_3$ and CCl_2F_2 with respect to the flow of $SiCl_4$. The desired percentage of the central core area was doped with Er ion through solution doping process and the rest portion remain undoped having the same refractive index value. From fabrication point of view, the critical steps involve to maintain the same refractive index value throughout the whole core region with and without Er ions. Second, to achieve the thickness of photo-sensitive layer around 2.75 micron under control of the flow of $SiCl_4$ with respect to $GeCl_4$ along with the number of deposition passes as well as proper control of the burner speed. Third, another critical step involve the doping of Er ions only 8 to 9% of the total core region of the proposed design based optical fiber. The parameter of proposed design of dual core Er doped fiber is given below.

Experimentally the area of the doped region within the whole core is found from electron probe microanalyses (EPMA) of PDCF preform shown in Fig. 1, where the

TABLE II
COMPOSITIONS OF UN-DOPED PHOTOSENSITIVE AND DOPED LAYERS OF PDCF

Composition of the undoped photo-sensitive core layer	Composition of the Er_2O_3 doped core layer
SiO_2-GeO_2	SiO_2-Al_2O_3-Er_2O_3
GeO_2:- 2.5 wt%	Al_2O_3:- 1.75 wt% , Er_2O_3 :- 0.5 wt% Er_2O_3:- 0.4 wt%

elemental analyses obtained through scanning along the whole diameter of the fiber preform section. The elemental analyses of the partially erbium doped core fiber preform sample is mentioned below where yellow area shown in the plot describe the undoped photosensitive region and red area signify the actual doping region of Er_2O_3 and Al_2O_3.

From the graph of EPMA of the fiber preform samples we are able to calculate the diameter of the whole core area and Er_2O_3 doped core region. Theoretically the total core and the doped core region are also obtained from the calculated thickness of the un doped and doped core with respect to the desired flow rates of $SiCl_4$, $GeCl_4$ against deposition of the sintered un-doped core layers and with respect to the flow rate of SiCl4, deposition temperature and the viscosity of the dopant precursor solution respectively.Theoretically the total core and the doped core region are also obtained from the calculated thickness of the un doped and doped core with respect to the desired flow rates of $SiCl_4$, $GeCl_4$ against deposition of the sintered un-doped core layers and with respect to the flow rate of $SiCl_4$, deposition temperature and the viscosity of the dopant precursor solution respectively. However the previous experimental process based on EPMA is found to be more accurate than the theoretical method. From EPMA analyses of such kind of erbium doped photosensitive fiber (EDPF) with double layers core structure, the total diameter of undoped photosensitive layer with doped layer is found to be around 9.5 micron Whereas the diameter of Er_2O_3 doped core is found to be around 4.0 micron. So the thickness of photo-sensitive layer around the central doped core is found to be around 2.75 micron. The doping level of Er ions is found to be around 400 ppm. The compositions of un-doped photosensitive and doped layers are given in the following table.

We have studied the geometrical and optical characterization of such kind of erbium doped photosensitive fiber. Refractive-Index profile of photosensitive erbium doped fiber is measured by Fiber Analyzer. The cross-section view and refractive index profile of the fiber is given in Fig. 2(a) and (b) respectively. The unit of y-axis is the refractive index difference with respect to pure silica glass.

The loss of such type of fiber is measured by cut-back method using Bentham Spectral attenuation set-up after splicing of the fiber with standard SMF and light is launched on such SMF. The spectral attenuation of the fiber is given in Fig. 3.

By comparison with depressed cladding erbium doped fiber where the entire core region is doped with erbium having depressed cladding structure containing 3% Fluorine, 0.5% P_2O_5 [17]. In PDCF structure the doped and undoped region was made with the same refractive index which serves as a whole core region. Here the active doped region is around 2.75 micron which become 40% of the total core region to get better overlapping of the Gaussian pump beam with the total active region. In this index profile structure, mode field distribution falls outside 60% remaining area of core region at the bending situation which gives rise more bending losses to show more sensitive compared to the depressed clad structure. Such structure will give more flexibility compared to the depressed clad structure proposed by [17]. From view point of fabrication as well as better overlapping of the fundamental propagation mode with the erbium doped region to get more bending sensitivity.

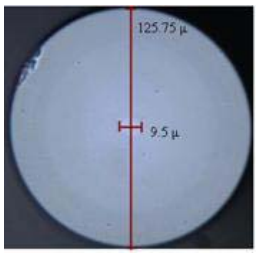

(a)

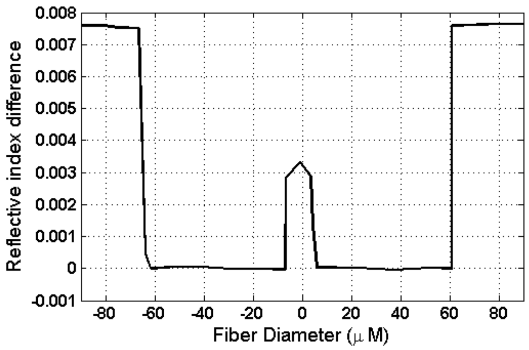

(b)

Fig. 2. (a) Cross-sectional view of photosensitive erbium doped fiber (PDCF). (b) Refractive-index profile of photosensitive erbium doped fiber with respect to pure silica glass (PDCF).

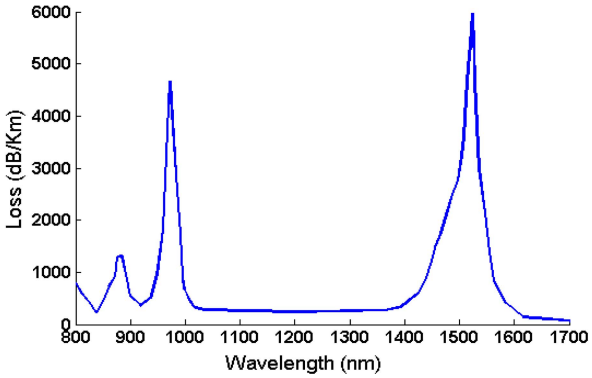

Fig. 3. Spectral attenuation of photosensitive erbium doped fiber (PDCF).

III. Principle of Macro-Bend PDCF Sensor

The overall loss in the macro-bend PDCF is represented by active bending loss and passive bending loss. Passive bending loss is related to macro-bending loss where the field distribution in the fiber is modified. On the other hand, the active bending loss relates to overlap difference of optical mode with the doped ions that will stimulate absorption and emission from erbium transitions. The effects of active and passive bending loss can be described by the coupled differential equation which is defined as follow [18], [19]

$$\frac{dP^{\mp}(\lambda)}{dz} = \Gamma(\lambda)P^{\pm}(\lambda)\sum_{ij}((N_i\sigma_{ij}(\lambda) - N_j\sigma_{ji}(\lambda))) \pm\Gamma(\lambda)\sum_{ij} 2hv_{ij}\Delta v\ n_{i_i}\sigma_{ij}(\lambda) \pm (\alpha_{P,s})P^{\pm}(\lambda) \quad (1)$$

Eq.1 describes the evolution of pump power (Pp), signal power (Ps) and ASE (Pase) along the doped fiber. The passive bending loss effects is reflected by $\alpha_{P,s}$ and the active bending loss effects is embedded in the overlap factor, $\Gamma(\lambda)$. Various mathematical models have been suggested to calculate the bending effects in optical waveguide [20]. Earlier references for bending loss at single mode fibers with step index profiles were developed by Marcuse [21]. According to Marcuse, the total loss of a macro bent fiber includes the pure bending loss and transition loss caused by mismatching between the quasi-mode of the bending fiber and the fundamental mode of the straight fiber [22]. The analytical expression for fiber bend loss α is expressed as follow [21]:

$$\alpha(v) = \frac{\sqrt{\pi}k^2\exp\left[-\frac{2}{3}\left(\gamma^3/\beta_g^2\right)R\right]}{e_v\gamma^{2/3}V^2\sqrt{R}K_{v-1}(\gamma a)K_{v+1}(\gamma a)} \quad (2)$$

where $e_v = 2$, a is the radius of fiber core, R is the bending radius, β_g is the propagation constant of the fundamental mode, $K_{v-1}(\gamma\alpha)$ and $K_{v+1}(\gamma\alpha)$ are the modified Bessel functions. The values of k and γ can be defined as follows [23]:

$$k = \sqrt{n_1^2k^2 - \beta_g^2} \quad (3)$$

$$\gamma = \sqrt{\beta_g^2 - n_2^2k^2} \quad (4)$$

For an optical fiber with length L, bending loss (α) is obtained by: $\alpha_L = 10\log(\exp(2\alpha L)) = 8.68\alpha L$ Eq. (3) agrees well with our earlier experimental results for macro-bent single-mode fiber [24], [25]. This mathematical model reflects what we introduce as passive bending loss in our model for macrobend PDCF.

The active bending loss is best reflected by the overlap factor, $\Gamma(\lambda)$ which is a measure of the portion of the optical mode which overlaps with the Thulium ion distribution that will stimulate absorption or emission from erbium transitions. The overlap factor equation is defined by [18]:

$$\Gamma(\lambda) = \frac{2\pi\int_0^{\infty}|E(r,\phi,\lambda)|^2 \times\ n_T(r)\times r\times dr}{N_T\int_0^{\infty}|E(r,\phi,\lambda)|^2\times r\times dr} \quad (5)$$

$n_T(r)$ and n_T are transverse distribution profile (TDP) of doped fiber amplifier (DFA) and total dopant concentration per unit per length defined by [12], [14]:

$$N_T = 2\pi\int_0^{\infty} n_T(r)\times r\times dr \quad n_T(r) = n_{T,\max}\times e^{-[|r-\delta|/\theta]^{\beta}} \quad (6)$$

where $n_{T,max}$ is the value of the maximum erbium concentration per unit volume and r is the radial coordinate. Variables θ, β and δ represent dopant radius, the roll off factor of the profile and the radial position of the profile peak, respectively. $|E(r,\phi,\lambda)|^2$ is the mode field intensity for guided mode. In order to calculate mode field intensity at different distribution profile in the bend fiber, the beam propagation method (BPM), was used. In BPM technique [26], the bent fiber is defined as a straight fiber with modified reflective index distribution along the core axis x as follows: [27]

$$n' = n_{material}e^{\left(\frac{x}{R}\right)} \approx\ n_{material}\left(1+\frac{x}{R}\right) \quad (7)$$

The physical refractive index of the fiber will change after the bending. This stress-optic effect causes the material refractive index distribution to change as follows:

$$n_{material} = n\left[1-\left(\frac{n^2x}{2R}\right)[P_{12}-v(P_{11}+P_{12})]\right] \quad (8)$$

where n is the refractive index of the straight fiber, P_{11} and P_{12} are components of the elasto-optical tensor. By combining equation (7) and (8), the modified refractive index of the bent fiber is:

$$n' = n\left(1+\frac{x}{R_{eff}}\right) \quad (9)$$

where R_{eff} is defined as:

$$R_{ef} \equiv \frac{R}{\frac{n^2}{2}[P_{12}-v(P_{11}+P_{12})]} \quad (10)$$

Fig. 4 displays an example of transversal mode field distribution of the fundamental mode when the doping radius is 2 μm and 4 μm (blue circles), core radius is fixed at 4 μm. To understand the longer wavelength suppression mechanism using macro bending approach, the transversal mode field distribution of the fundamental mode at two different wavelengths (1560 nm, 1800 nm) for both straight and bent fiber are investigated The transversal mode field distribution of straight fiber and bent fibers are shown at left and right columns respectively. The fiber used has a nA of 0.0927. Figs. 4(a) and (b) show the mode field distribution for LP01 mode at 1560 nm for the straight and bent fiber with doping radius of 4 μm, respectively. Fig. 4(c) and (d) show the same distribution for 1800 nm operation. It is found that the LP01 mode at shorter wavelength region of 1560 nm is not significantly affected as compared to 1800 nm region. This is attributed to the 1560 nm signal, which has a smaller MFD, calculated to be 13.971 μm, and thus the propagating light is tightly confined in the core. At 1800 nm, the MFD is 22.461 μm, which leads to poor light confinement [28], [29]. Higher MFD at longer wavelength

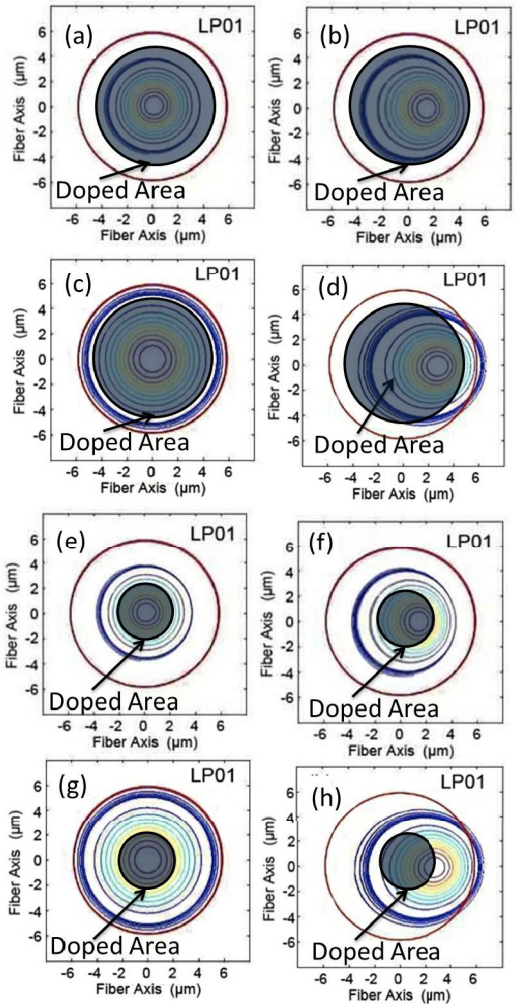

Fig. 4. LP01 Transversal mode field distribution. (a) 4 μm doped EDFA at 1560 nm (straight fiber), (b) 4 μm doped EDFA at 1560 nm (bent fiber). (c) 4 μm doped EDFA at 1800 nm (straight fiber), (d) 4 μm doped EDFA at 1800 nm (bent fiber), (e) 2 μm doped EDFA at 1560 nm (straight fiber), (f) 2 μm doped EDFA at 1560 nm (bent fiber), (g) 2 μm doped EDFA at 1800 nm (straight fiber), and (h) 2 μm doped EDFA at 1800 nm (bent fiber).

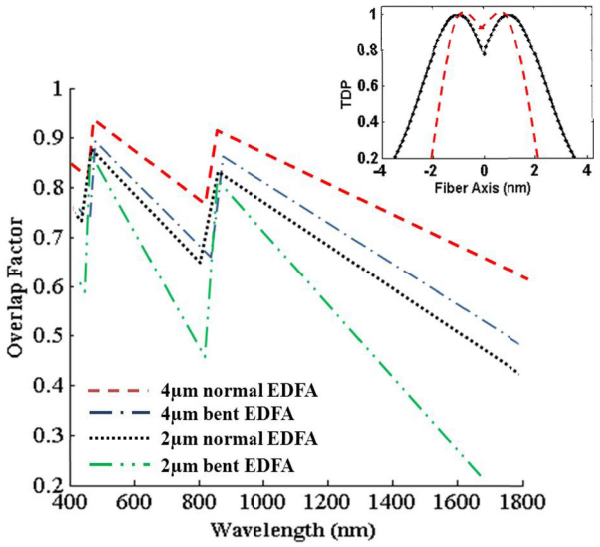

Fig. 5. 4 μm and 2 μm co-doped fibers overlap factor vs wavelength for normal and bent conditions.

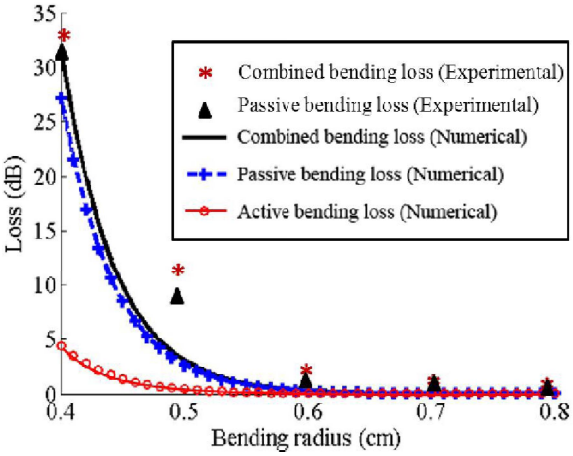

Fig. 6. 4 μm doping radius fiber bent EDFA attenuation numerical and experimental result.

leads to higher bending loss as the fiber bending radius reduces. Fig. 4(e) and (f) show the mode field distribution for LP01 mode at 1560 nm for the straight and bent fiber with doping radius of 2 μm. Fig. 4(c) and (d) show the same distribution for 1800 nm operation. The mode field distribution for 2 μm radius doped fiber in comparison with 4 μm radius doped fiber falls outside the doping area at the bending situation and suffers more due to active bending loss. Typical curve of $\Gamma(\lambda)$ for normal and bent conditions of PDCF with optimized core radius of 4 μm, for 4 μm and 2 μm doping radius are shown in Fig. 5. The bending radius for 4 μm and 2 μm doping radius fibers was fixed at 0.5 and 15 cm respectively. In the simulation, dopant distribution profile parameters are set as $\theta = 2$, $\beta = 1.5$ and $\delta = 0.1$ for 2 μm doping radius. For 4 μm doping radius, dopant distribution profile parameters are set as $\theta = 4$, $\beta = 4$ and $\delta = 0.8$. Both the dopant distribution profiles are shown in Fig. 5 inset. The overlap between guided mode and doped region in normal fiber is higher compared to bent fiber. For 2 μm doping radius, the overlap factor reduces drastically at longer wavelengths. This is due to the larger MFD, which then reduces the overlap. The reduction in overlap factor at longer wavelengths is also observed in 4 μm doping radius but at a reduced slope. This is due to a larger doping region that allows greater overlap compared to the 2 μm doping radius fiber. The discontinuity at 480 nm and 800 nm is a result of transition of $LP_{12}$and LP_{11}higher order mode. In order to show the effect of Active Bending Loss (ABL) and Passive Bending Loss (PBL) the numerical model of PDCF for 4 μm and 2 μm doping radius fibers was developed. As described before, the overall loss in the bent PDCF is represented as Combined Bending Loss ($\chi_{P,s}$) which is a combination of Active Bending Loss ($\gamma_{P,S}$) and Passive Bending Loss (α_L). In our numerical model the passive bending loss was calculated form equation 2 and the combined bending loss was calculated based on equation 1 by subtract the gain variation of straight and bent fiber. So the active bending loss can be calculated from $\gamma_{P,S} = \chi_{P,s} - \alpha_L$. Figs. 6 and 7 illustrate the modeling

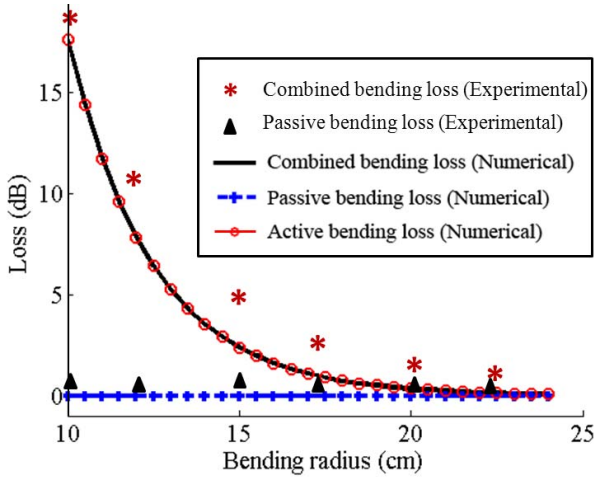

Fig. 7. 2 μm doping radius fiber bent EDFA attenuation numerical and experimental result.

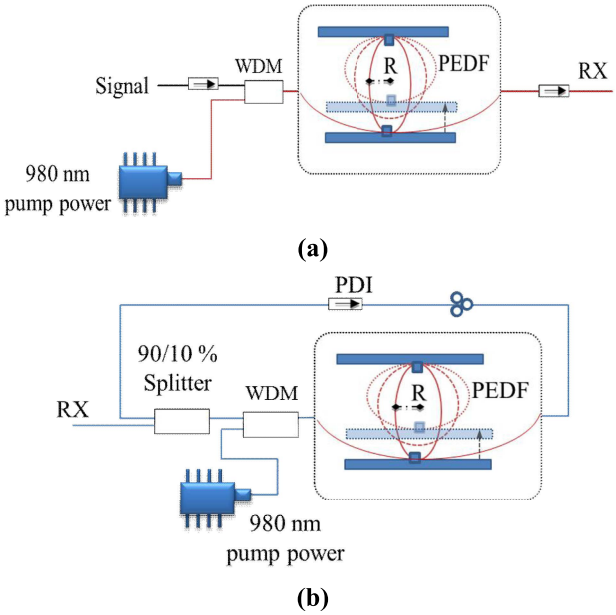

Fig. 8. PDCFA as sensor used in (a) ASE sensor and (b) laser sensor (ring laser).

and experimental results of $\chi_{P,s}$, $\gamma_{P,S}$ and α_L losses for 4 μm and 2 μm doping radius respectively. The fiber length is set at 1 m and the wavelength is fixed at 1540 nm. At bending radius lower than 0.5 cm higher passive bending loss is achieved rather than active bending loss for 4 μm doped fiber. With agreement to Figs. 4 and 5, combined bending loss ($\chi_{P,s}$) are mainly from passive bending loss (α_L) at larger doping radius. By decreasing the doping radius to 2 μm the active bending loss increase significantly to about 18 dB at 100 mm bending radius. The passive bending loss still remains zero at above 6 mm bending radius. The fiber combined bending loss is measured experimentally by subtracting the gain variation of straight and bent fiber in pumped situation. The passive bending loss was measured by measurement of loss in un-pumped fiber. The good trend agreement between experimental and numerical results verifies the proposed model.

IV. Experimental Setup

The basic configurations of the PDCF sensor used in this work are depicted in Fig. 8(a) and (b), namely an amplifier and fiber laser respectively. The experimental setup was done based on [10], [11]. In Fig. 8(a) the PDCF amplifier sensor is used as a single pass amplifier. The PDCF amplifier is pumped by a 980 nm laser diode operating at 50 mW. We measured the output signal using an OSA by changing the PDCF bending radius (R) using one calibrated metallic mandrill. In the reference position we measured the ASE and subsequently calibrate the sensor by changing the PDCF bending radius (R) using a calibrated compression setup. The main mechanism of sensing for proposed amplifier sensor is the longer wavelength suppression and gain shifting to shorter wavelength by bending the fiber. Since in standard EDF, the longer wavelengths are not suppressed, in PDCF the longer wavelength suppression process is improved and is used as the bending sensor. Another setup for the sensor is show in Fig. 8(b), where the PDCF sensor used in a ring fiber laser. An optical 90%/10% splitter was used at the sensing system output to obtain a sample laser light and to connect the counter-propagating ASE power generated by the near end PDCF (90% port) in to the far end of PDCF. The polarizing isolator lets the central intense part of the pulse pass but blocks (absorbs) the low-intensity pulse wings. The net result is that the pulse is slightly shortened after one round trip inside the ring cavity, an effect identical to that produced by a fast saturable absorber. In other words, the polarization dependent isolator, working together with the birefringence fibers generates an intensity-dependent loss mechanism in the cavity that contributes to mode-locked square pulse generation. The mechanism of sensing for proposed fiber laser sensor is the same as amplifier where the longer wavelength suppression leads to wavelength peak shifting to shorter wavelength. By increasing the bending radius, the higher fiber loss at longer wavelength shifts the lasing wavelength to shorter wavelengths.

V. Experimental Results and Discussion

Fig. 9 shows the ASE spectrum level with respect to different mandrill radius (R). The optimize PDCF length was set 5 m long. When the fiber is unspooled, the emitted ASE spectrum gives an output wavelength that peaked at 1539 taken at an output power level of about -38 dBm. The peak power of the ASE spectrum remains constant when the PDCF mandrill radius decreases up to 20 cm. When the PDCF is being compress into smaller radius, the peak power level of the ASE spectrum, with the centre wavelength are changed. As can be seen from the Fig. 9, the ASE power level decrease and peak wavelength of the ASE spectrum shift to shorter wavelength with the decrease of the EDF mandrill radius. The ASE power level from -38.0 dBm to -61.8 dBm as the spooling radius is reduced from 20 cm to 3 cm due to higher bending loss at smaller mandrill bending radius as expected from Fig. 5. The dash line shows the peak wavelength variation as a function of bent radius. As expected from overlap factor

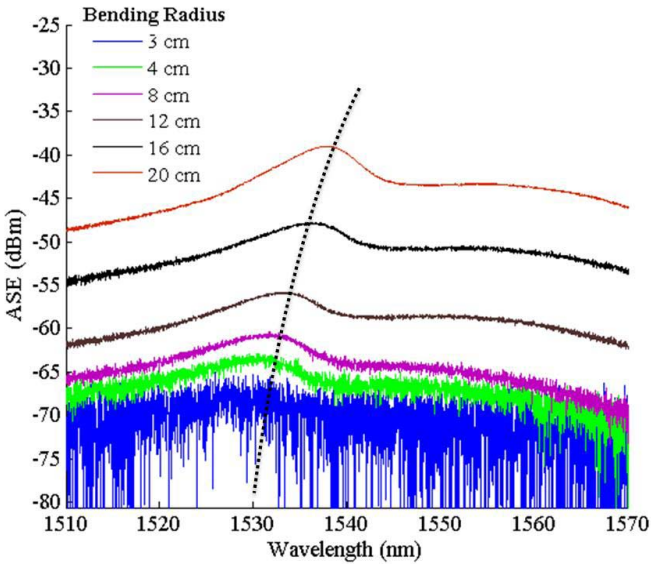

Fig. 9. ASE power in the amplifier sensor output, with different bending radius.

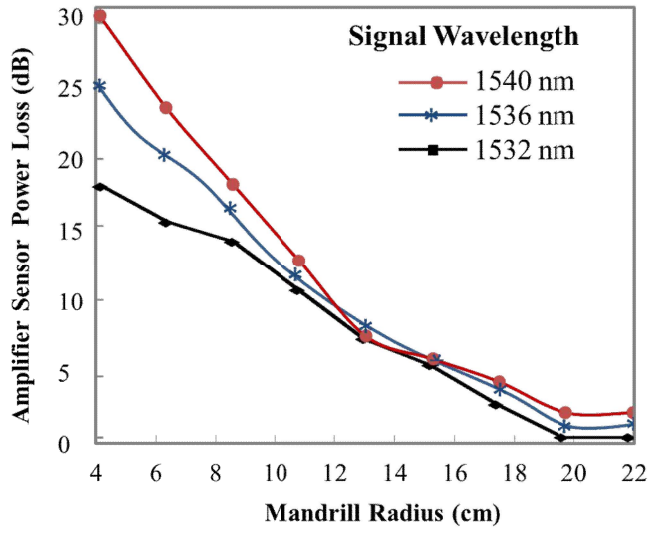

Fig. 10. The amplifier sensor peak power loss for 1532 nm, 1536 nm and 1540 nm wavelength versus different bending radius.

spectrum (Fig. 6) as the spooling radius is reduced the longer wavelength suppression is increase due to higher MFD at longer wavelength. These phenomena lead the gain peak shift from 1538 nm to 1530 nm with respect to the decrease of the spooling radius from 20 cm to 3 cm. This is the principle of operation behind the ASE based PDCF sensor.

We also analyzed the the PDCF amplifier loss variation comparing between bending and non-bending behavior at three different wavelengths of 1532 nm,1536 nm and 1540 nm as shown in Fig. 10. The bending loss is the optical power measured without bending the PCDFA, minus the optical power measured at different mandrill radius (R). In this case, the DC-EDF was always pumped. The 980 nm pump power fixed at 70 mw and input signal power is −30 dBm respectively. The 8 m optimized length of PDCF is achieved at selected pump

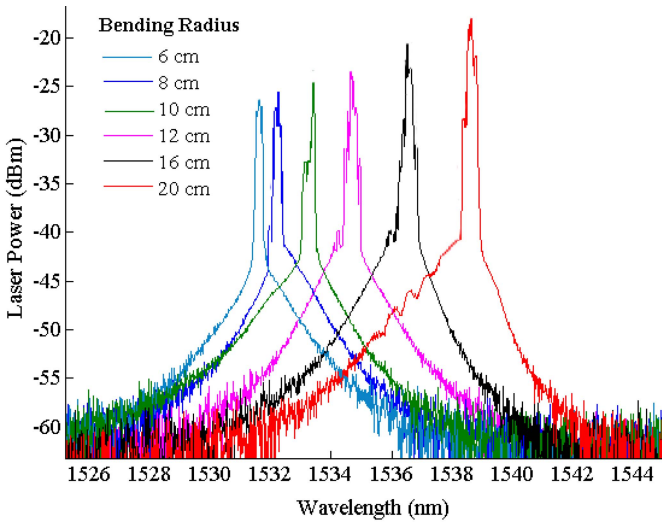

Fig. 11. Laser output in the laser sensor output, with different bending radius.

power. As expected from ASE spectrum major loss variation is for 1540-nm signal due to higher loss for higher MFD at longer wavelength. This bending radius variation range is a good choice to sensing static parameters such as forces, pressure and displacement. Observing Figs. 6 and 9, it is possible to affirm that the performance of the 1532 nm signal in terms of loss variation improves for a bending radius lower than 10 cm because the beam intensity more intense within the core. The loss variation of 30 dB for 8 m PCFA length obtained for 1540 nm signal in the range from 4 to 20 cm bending radius is better when compared with the best bending sensor introduced so far. For example in [10] and [11], Rosolem *et. al.*, showed the fiber loss variation of 43 dB for the bending radius range from 1.8 to 3.8 cm bending radius using depressed cladding erbium doped fiber amplifier.

The mode locked fiber laser PDCF sensor can be designed in the same rules of ASE PDCF sensor. Since the feedback loop shown in Fig. 4(b) provides enough ASE power, the ring laser will oscillate in the tuned locked frequencies. Fig. 11 shows some experimental tuned ring laser spectral lines of the laser sensor used in this work. In this case, the optimized PDCF length was 8 m long and spooled in a loop radius from 6 cm to 20 cm. As expected from ASE peaks variation the spectral operation is changed from 1539 nm to 1530 nm range. This phenomenon occurs due to higher MFD of longer wavelength and result of optical filtering at longer wavelengths.The relationship between the bending radius and the operating wavelength for Mode lock fiber laser and the amplifier peak power loss for amplifier sensor showed that, the laser operating wavelength locked to shorter wavelength exponentially with the increase of the bending diameter due to longer wavelength ASE suppression.

Finally, for the best of our knowledge, the comparisons between different EDFA structures namely normal EDFA, DC-EDFA and PDCF demonstrated in Table III. It is shown that the C-band operation, high threshold bending radius of 20 mm and high ranges of bending radius operation are the most eminent advantages of PDCF. In PDCF ASE based

TABLE III
COMPARISONS BETWEEN DIFFERENT EDFA STRUCTURES

	EDFA	DC- EDFA		PDCF	
	Amplifier	Amplifier	Laser	Amplifier	Laser
Reference	[15]	[10]	[11]	[16]	
Operating band	C-band	S-band	S-band	C-band	C-band
Operating bend radius ranges (mm)	0.4~0.8	7.5~53	16 ~34	30~200	60~200
ASE power variation	-5 ~ -30 dBm	-5 ~ -30 dBm	-15~-20 dBm	-38~-61.8 dBm	-18~-28 dBm
Peak power loss (dB)	0-30 (dB)	0-35 (dB)	NA	0-30	NA
Wavelength Peak shift ranges	1530~1530	1450~1490	1495~1515	1530~1540	1530 ~1539
Bending effects threshold (mm)	0.4	7.5	16	30	60
Sensitivity based on power loss (dB/mm)	2	35	NA	0.25	NA
Sensitivity based on peak wavelength shift (nm/mm)	0	0.86	1.1	0.5	0.7
Temperature Sensitivity (dB/ºC)	0.05	NA	NA	0.005	0.005

sensor, the ASE power level will change from -38.0 dBm to -61.8 dBm as the spooling radius is reduced from 20 cm to 3 cm is measured. The 0.25 dB/mm sensor sensitivity based on power loss is was achieved in PCDF amplifier. On the other hand, in DC-EDFA, ASE power level will change from -30.0 dBm to -5 dBm as the spooling radius is reduced from 20 cm to 3 cm. the sensor sensitivity of 35 dB/mm was achieved in DC- EDFA sensor. As expected from PCDF amplifier sensor peak variation, the mode lock fiber laser sensor spectral operation is changed from 1539 nm to 1530 nm range. The 0.7 dB/nm sensor sensitivity based on peak wavelength is was achieved in PCDF mode lock fibre laser.

Stability measurement of the fiber laser sensor from the PDCF is carried out within 60 minutes of observation time with an interval of 5 minutes between the measured outputs. This measurement is taken with the PDCF in spooled position. With an interval of 5 minutes, the output spectrum of the ASE is observed to be constant for the 60 minutes observation time. No significant variation is observed in terms of the output power and the output operating wavelength.

VI. CONCLUSION

In this paper, a novel Partially Doped Core Fiber (PDCF) for high sensitive bend sensor is proposed and demonstrated. The fabrication method of PDCF with un-doped outer region of about 9.5 μm and inner core region of about 4.00 μm with an Er_2O_3 dopant concentration of 400 ppm is demonstrated. The mechanism of bending effect in proposed PDCF is explained. The amplifier PDCF B is pumped by a 980 nm laser diode. In the case of ASE based sensor, the ASE power level from -38.0 dBm to -61.8 dBm as the spooling radius is reduced from 20 cm to 3 cm is measured. The gain peak shift from 1538 nm to 1530 nm with respect to the decrease of the spooling radius from 20 cm to 3 cm due to higher bending loss at smaller bending radius as expected from overlap factor of PDCF is observed. As expected from ASE peak variation, the fiber laser sensor spectral operation is changed from 1539 nm to 1530 nm range. This is due to higher MFD of longer wavelength and result of optical filtering at longer wavelengths. The output of the ASE is also highly stable, with no observable variation in the power output over a measurement period of one hour.

REFERENCES

[1] K. Grattan and T. Sun, "Fiber optic sensor technology: An overview," *Sens. Actuators A, Phys.*, vol. 82, nos. 1–3, pp. 40–61, 2000.

[2] B. Culshaw and A. Kersey, "Fiber-optic sensing: A historical perspective," *J. Lightw. Technol.*, vol. 26, no. 9, pp. 1064–1078, May 1, 2008.

[3] H. N. Li, D. S. Li, and G. B. Song, "Recent applications of fiber optic sensors to health monitoring in civil engineering," *Eng. Struct.*, vol. 26, pp. 1647–1657, Sep. 2004.

[4] B. Xu, Y. Li, M. Sun, Z. W. Zhang, X. Y. Dong, Z. X. Zhang, *et al.*, "Acoustic vibration sensor based on nonadiabatic tapered fibers," *Opt. Lett.*, vol. 37, pp. 4768–4770, Nov. 2012.

[5] S. K. Yao and C. Asawa, "Fiber optical intensity sensors," *IEEE J. Sel. Areas Commun.*, vol. 1, no. 3, pp. 562–575, Apr. 1983.

[6] A. Vijayan, S. Gawli, A. Kulkarni, R. Karekar, and R. Aiyer, "An optical fiber weighing sensor based on bending," *Meas. Sci. Technol.*, vol. 19, no. 10, p. 105302, 2008.

[7] W. Liu, T. Guo, A. C. Wong, H. Y. Tam, and S. He, "Highly sensitive bending sensor based on Er^{3+}-doped DBR fiber laser," *Opt. Exp.*, vol. 18, pp. 17834–17840, Aug. 2010.

[8] S. Idris, F. Abdullah, M. Al-Mansoori, M. Jamaludin, and N. Din, "Pressure sensing utilizing linear cavity erbium-doped fiber laser," *Laser Phys.*, vol. 20, no. 4, pp. 855–858, 2010.

[9] P. K. Y. Ko, S. Demokan, and H. Tam, "Distributed temperature sensing with erbium-doped fiber amplifiers," *J. Lightw. Technol.*, vol. 14, no. 10, pp. 2236–2245, Oct. 1996.

[10] J. B. Rosolem, M. B. Elias, E. W. Bezerra, and C. K. Suzuki, "Bending sensor based on *S*-band depressed cladding erbium-doped fiber," *IEEE Photon. Technol. Lett.*, vol. 22, no. 14, pp. 1060–1062, Jul. 15, 2010.

[11] J. B. Rosolem, M. B. Elias, L. A. Ribeiro, and C. K. Suzuki, "Optical sensing systems based on depressed cladding erbium doped fiber," *J. Lightw. Technol.*, vol. 30, no. 8, pp. 1190–1195, Apr. 15, 2012.

[12] S. D. Emami, H. A. Abdul-Rashid, H. Ahmad, A. Ahmadi, and S. W. Harun, "Effect of transverse distribution profile of thulium on the performance of thulium-doped fibre amplifiers," *Ukrainian J. Phys. Opt.*, vol. 13, pp. 74–81, 2012.

[13] E. Desurvire, *Erbium-Doped Fiber Amplifiers: Principles and Applications*. New York, NY, USA: Wiley, 1994.

[14] J. C. Martin, "Erbium transversal distribution influence on the effectiveness of a doped fiber: Optimization of its performance," *Opt. Commun.*, vol. 194, pp. 331–339, Jul. 2001.

[15] S. D. Emami, H. A. Abdul Rashid, S. E. Mirnia, A. Zarei, S. W. Harun, and H. Ahmad, *Selected Topics on Optical Amplifiers in Present Scenario*. Rijeka, Croatia: Intech, 2013.

[16] H. Ahmad, M. Zulkifli, F. Muhammad, J. Samangun, H. Abdul-Rashid, and S. Harun, "Temperature-insensitive bend sensor using entirely centered erbium doping in the fiber core," *Sensors*, vol. 13, no. 7, pp. 9536–9546, 2013.

[17] M. A. Arbore, Y. Zhou, Y. Keaton, and T. Kane, "36 dB gain in S-band EDFA with distributed ASE suppression," in *Proc. Opt. Amplif. Appl.*, Vancouver, BC, Canada, 2002, pp. 1–3.

[18] S. D. Emami, H. A. A. Rashid, S. Z. M. Yasin, K. A. M. Shariff, M. I. Zulkifli, Z. Yusoff, *et al.*, "New design of a thulium–aluminum-doped fiber amplifier based on macro-bending approach," *J. Lightw. Technol.*, vol. 30, no. 20, pp. 3263–3272, Oct. 15, 2012.

[19] S. D. Emami, *Thulium Doped Fiber Amplifier, Numerical and Experimental Approach*. Commack, NY, USA: Nova, 2011.

[20] Q. Wang, G. Farrell, and T. Freir, "Theoretical and experimental investigations of macro-bend losses for standard single mode fibers," *Opt. Exp.*, vol. 13, pp. 4476–4484, Jun. 2005.

[21] D. Marcuse, "Curvature loss formula for optical fibers," *J. Opt. Soc. Amer. B*, vol. 66, no. 3, pp. 216–220, 1976.

[22] D. Marcuse, "Field deformation and loss caused by curvature of optical fibers," *J. Opt. Soc. Amer.*, vol. 66, pp. 311–320, 1976.

[23] D. Marcuse, *Light Transmission Optics*, 2nd ed. New York, NY, USA: Van Nostrand Reinhold, 1982.

[24] S. A. Daud, S. D. Emami, K. S. Mohamed, N. M. Yusoff, L. Aminudin, H. H. Abdul-Rashid, *et al.*, "Gain and noise figure improvements in a shorter wavelength region of EDFA using a macrobending approach," *Laser Phys.*, vol. 18, pp. 1362–1364, Nov. 2008.

[25] S. A. Daud, S. D. Emami, K. S. Mohamed, H. A. Abdul-Rashid, S. W. Harun, H. Ahmad, *et al.*, "Shorter wavelength gain shift in EDFA using a macro-bending approach," in *Proc. IEEE IPGC*, vols. 1–2. Dec. 2008, pp. 412–414.

[26] K. Kawano and T. Kitoh, *Introduction to Optical Waveguide Analysis: Solving Maxwell's Equations and the Schrodinger Equation*. New York, NY, USA: Wiley, 2001.

[27] R. T. Schermer and J. H. Cole, "Improved bend loss formula verified for optical fiber by simulation and experiment," *IEEE J. Quantum Electron.*, vol. 43, no. 10, pp. 899–909, Oct. 2007.

[28] G. P. Agrawal, *Fiber-Optic Communication Systems*, 2nd ed. New York, NY, USA: Wiley, 1997.

[29] D. Marcuse, "Loss analysis of single-mode fiber splices," *Bell Syst. Tech. J.*, vol. 56, no. 5, pp. 703–718, 1977.

Siamak Dawazdah Emami received the Degree in electronics engineering from Bushehr University, and the master's degree in electrical engineering from the University Malaya, Malaysia, in 2010, where he is currently pursuing the Ph.D. degree. His research relates to modeling of doped fiber amplifiers and all optical OFDM transmission system.

Hairul A. Abdul-Rashid received the B.Eng. degree in electrical and electronic engineering from University College London in 1997 and the M.Eng.Sc. degree in signal processing from Multimedia University in 2002, and the Ph.D. degree optical communication systems from Multimedia University in 2007. He has been with the Faculty of Engineering, Multimedia University since 1998. He is currently a Lecturer at the faculty besides leading a research team at the Center for Photonics and Electronic Devices in specialty fiber fabrication, optical amplifiers, fiber sensors, and fiber lasers.

Fatemeh Zahra Zahedi received the B.S. degree in computer engineering from the K. N. Toosi University of Technology, Tehran, Iran, in 2010, and the M.Eng.Sc. degree from the Electrical Engineering Department, University of Malaya, Kuala Lumpur, Malaysia, in 2012. She is currently pursuing the Ph.D. degree in telecommunication engineering at Shahid Beheshti University, Tehran.

Mukul Chandra Paul received the M.Sc. degree in inorganic chemistry from Burdwan University in 1989 and the Ph.D. degree in radiation sensitive fibers for evaluation of their radiation response behavior at room temperature from the Central Glass and Ceramic Research Institute in 2003. Since 1997, he has been a Research Scientist with the Fiber Optics and Photonics Division, CGCRI. He has authored or co-authored more than 100 scientific articles in journal and conference proceedings and holds four U.S. patents on fabrication of rare-earth doped fibers. He is a member of the Optical Society of America and a Life Member of the Material Research Society of India and Indian Ceramic Society. He is an Editorial Board Member of the *New Journal of Glass and Ceramics (NJGC)*. His current research interests include suitable crystalline host based PS fibers for writing FBGs and advanced rare earth doped nano-engineering host based optical fibers for high power fiber laser and up-conversion laser, and metal and transition elements doped nano-crystalline fiber for low-threshold super-continuum generation.

Shyamal Das received the B.E. and M.E. degrees in chemical engineering from Jadavpur University. He has five years of research experience in sol gel processing. He joined the Fiber Optics and Photonics Group in 2006. He is working on fabrication of radiation sensitive fiber, Er doped fiber, large fiattened mode fiber, thulium doped fiber, and specialty optical fiber.

Mrinmay Pal received the Ph.D. degree in specialty erbium-doped fiber for broad-band amplification and gain-flattened optical amplifiers for WDM network systems. His research has primarily focused on development of optical fiber amplifiers, lasers, and PCF. He has worked on the development of EDFA for CATV and DWDM applications with industrial collaboration. He is currently involved in fiber laser and supercontinuum generation. He has authored or co-authored 20 scientific articles in journal and conference proceedings and holds two U.S. patents on fabrication of rare-earth doped fibers. He is a member of the Optical Society of America in 2006 and a Life Member of the Optical Society of India.

Sulaiman Wadi Harun received the B.E. degree in electrical and electronics system engineering from the Nagaoka University of Technology, Japan, in 1996, and the M.Sc. and Ph.D. degrees in photonics from the University of Malaya in 2001 and 2004, respectively. Currently, he is a Full Professor with the Faculty of Engineering, University of Malaya. His research interests include fiber optic active and passive devices.